Mn 2+ bispidine complex combining exceptional stability, inertness and MRI efficiency

Daouda Ndiaye, Patrick Cieslik, Hubert Wadepohl, Agnès Pallier, Sandra Même, Peter Comba, Éva Tóth

Mn^{2+} bispidine complex combining exceptional stability, inertness and MRI efficiency

Daouda Ndiaye,[a)‡] Patrick Cieslik,[b)‡] Hubert Wadepohl,[b)] Agnès Pallier,[a)] Sandra Même,[a)] Peter Comba,[b,c)*] and Éva Tóth[a)*]

a) Centre de Biophysique Moléculaire, CNRS UPR 4301, Université d'Orléans, rue Charles Sadron, 45071 Orléans, France

b) Universität Heidelberg, Anorganisch-Chemisches Institut, INF 270, D-69120 Heidelberg, Germany

c) Universität Heidelberg, Interdisciplinary Center for Scientific Computing, INF 205, D-69120 Heidelberg, Germany

ABSTRACT. As an essential metal ion and an efficient relaxation agent, Mn^{2+} holds great promise to replace Gd^{3+} in MRI contrast agent applications, if its stable and inert complexation can be achieved. Towards this goal, four pyridine and one carboxylate pendants have been introduced in coordinating positions on the bispidine platform to yield ligand L^3. Thanks to its rigid and preorganized structure and perfect size-match for Mn^{2+}, L^3 provides remarkably high thermodynamic stability ($\log K_{MnL}$ = 19.47), selectivity over the major biological competitor Zn^{2+} (K_{MnL}/K_{ZnL} = 4.4), and kinetic inertness. Solid-state X-ray data show that $[MnL^3(MeOH)](OTf)_2$ has an unusual eight-coordinate structure with a coordinated solvent molecule, in contrast to the six-coordinate structure of $[ZnL^3](OTf)$, underlining that the coordination cavity is perfectly adapted for Mn^{2+}, while it is too large for Zn^{2+}. In aqueous solution, ^{17}O NMR data evidence one inner sphere water and dissociatively activated water exchange ($k_{ex}^{298} = 13.5 \times 10^7\ s^{-1}$) for MnL^3. Its water proton relaxivity (r_1 = 4.44 $mM^{-1}s^{-1}$ at 25 °C, 20 MHz) is about 30% higher than values for typical monohydrated Mn^{2+} complexes, which is related to its higher molecular size; its relaxation efficiency is similar to that of clinically used Gd^{3+}-based agents. *In vivo* MRI experiments realized in control mice at 0.02 mmol/kg injected dose indicate good signal enhancement in the kidneys and fast renal clearance. Taken together, MnL^3 is the first chelate that combines such excellent stability, selectivity, inertness and relaxation properties, all of primary importance for MRI use.

INTRODUCTION

For more than three decades, complexes of the paramagnetic Gd^{3+} ion have been extensively used as contrast agents and have largely contributed to the clinical success of Magnetic Resonance Imaging (MRI). Recently, safety concerns related to the use of Gd^{3+}-based agents[1-2] and the observation of small Gd-deposits in the brain and other tissues[3-4] have promoted increasing efforts towards safer and biocompatible alternatives.[5] Among these, complexes of Mn^{2+} are particularly promising.[6-18] Manganese is an essential metal ion and in the divalent state is a strong relaxing agent, due to five unpaired electrons, slow electron spin relaxation and generally fast water exchange.[19] Given the high concentrations needed for MRI contrast agents, the Mn^{2+} ion needs to be chelated with high stability and inertness of the complex in order to prevent free metal ion release even in a chemically challenging biological environment. In addition, the complex must contain at least one water molecule in the inner coordination sphere for good relaxation efficiency. In order to be considered as a viable replacement for current small molecular weight Gd^{3+} based agents, an Mn^{2+} probe should have comparable relaxivity at imaging fields, which is challenging given the lower spin (S=5/2) of Mn^{2+} with respect to Gd^{3+} (S=7/2). Finally, the contrast agent should easily distribute into the extravascular and extracellular space and have fast, mainly renal clearance.

Among the major ligand classes investigated for Mn^{2+} complexation in the context of MRI contrast agent development, open-chain chelators based on the *trans*-1,2-cyclohexylene backbone such as PyC3A and its derivatives,[6, 18] and ligands derived from the macrocyclic PC2A[8, 20-21] or *cis*-1,4-DO2A[22-23] proved to be the most promising (Scheme 1). Several of these complexes have passed the first *in vivo* MRI evaluation steps in preclinical models and MnPyC3A has just entered clinical trials.[24]

However, strong Mn^{2+} complexation remains challenging since Mn^{2+} complexes are typically labile. Due to the spherical *d* electron distribution leading to the Irving-Williams order of thermodynamic stability constants ($Mn^{2+} < Fe^{2+} < Co^{2+} < Ni^{2+} < Cu^{2+} > Zn^{2+}$), there generally is a lower stability for a Mn^{2+} complex than for its analogue formed with Zn^{2+}, the major divalent competitor in biological systems. We have recently identified the very first ligands based on a bispidine platform that are capable of providing selectivity for Mn^{2+} vs Zn^{2+} (L^1 and L^2 in Scheme 1; K_{MnL}/K_{ZnL} of 10^8-10^{10}).[25] These peculiar properties result from the remarkably rigid and large coordination cavity and the high denticity of these ligands that perfectly match the larger size of the Mn^{2+} ion (~10%), while they are less adapted to the smaller Zn^{2+}, which cannot accommodate all ligand donor groups. The difference in coordination geometry was evidenced by solid state crystal structures of the Mn^{2+} and Zn^{2+} complexes, DFT calculations, as well as solution studies. Both bispidine ligands form six-coordinate Zn^{2+} and rather unusual eight-coordinate Mn^{2+} complexes.

The bispidine L^4 [26] with the same rigid cavity as L^1-L^3 but a lower denticity (5 vs 7 or 8), as well as analogues of L^4,[27] provide a significantly lower complex stability ($\log K$ approx. 12 vs >20) and no

Mn^{2+} selectivity (K_{MnL}/K_{ZnL}=4×10^{-4}). However, MnL^4 is exceptionally inert, similarly to MnL^1. The lack of transmetallation is probably related to the rigidity of the bispidine backbone.[28-29]

We report here the new bispidine L^3 and its $[MnL^3(H_2O)]^+$ complex with chemical design elements that help fulfil requirements for a safe and efficient MRI contrast agent, i.e. high complex stability, Mn^{2+}/Zn^{2+} selectivity, resistance to dissociation together with excellent relaxation efficacy and water solubility. The four pyridine pendants on the bispidine backbone are expected to maintain a large coordination cavity, leading to high Mn^{2+} complex stability and good Mn^{2+}/Zn^{2+} selectivity, while the introduction of a carboxylate function increases water solubility. The elevated molecular weight of the ligand and complex (M_w = 676 g mol^{-1}) compared to typical Mn^{2+} based relaxation agents should result in increased relaxivity, comparable to that of clinically used Gd^{3+} agents, and thus ensuring good MRI contrast enhancement *in vivo*.

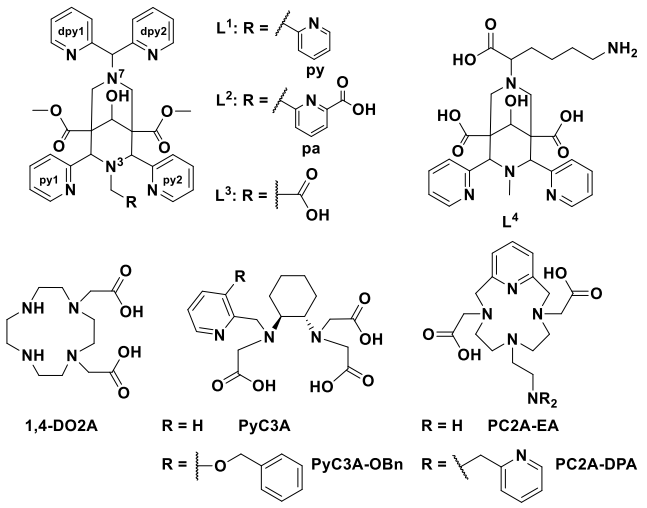

Scheme 1. Ligands discussed in the text.

RESULTS AND DISCUSSION

Synthesis and structural properties of MnL^3 and ZnL^3

Ligand L^3 was synthesized by a modified protocol starting from bispidine fragment 1 (Scheme 2; see Supporting Information for details). After alkylation with *tert*-butyl bromoacetate and subsequent deprotection, reaction with 2,2'-dipyridylmethylene chloride in the presence of Cs_2CO_3 formed L^3 in moderate yields. The Mn^{2+} and Zn^{2+} complexes were prepared in stoichiometric reactions of the ligand with the respective triflate salts in methanol. Ether diffusion yielded crystals suitable for X-ray structure determination. Selected bond lengths and angles are listed in Table 1 alongside with the data for MnL^1 and MnL^2, and plots of the molecular cations are presented in Figure 1.

As expected from previous work, L^3 perfectly wraps around the Mn^{2+} center, coordinating with all seven donor atoms. A methanol solvent molecule is also coordinated, ultimately leading to a rare example of an octacoordinate Mn^{2+} center.[25, 30-33] The coordinated ligand is protonated at the acetate appended to N3 – this follows from the stoichiometry ($[MnL^3(MeOH)](OTf)_2$) and the bond distances of the coordinated acetate group (the coordinated carbonyl oxygen to carbon bond is shorter than the protonated carboxylate to carbon bond, see Supporting Information). The situation in aqueous solution at physiological pH obviously is different, see potentiometric titration data below. In comparison to the complexes of L^1 and L^2, MnL^3 is more symmetrical: the metal-donor distances range from 2.182 – 2.621 Å and the elongation of one of the Mn^{2+}-pyridine bonds found in the structures with L^1 and L^2 is absent (see Table 1). This might be due to a combination of steric and electronic effects and is presumably also related to the protonated acetate arm, i.e. for the solution studies (see below) this is not relevant, at least at physiological pH. The coordination geometries of the three MnL^{1-3} complexes are similar, as seen in the overlay plot in Figure 1c. It is of no surprise either that the reaction of L^3 with Zn^{2+} yields a hexacoordinate structure, where one pyridine donor (Ndpy2) is dangling (Figure 1b), and this also emerges from the potentiometric titrations (see below; note that various close to degenerate isomers with six-fold coordination of the seven- and eight-dentate bispidines L are possible[25] and the pH titrations suggest that a tertiary amine is protonated). To confirm the ideal fit of the Mn^{2+} ion in the bispidine cavity, hole-size calculations were conducted (see Supporting Information for details),[34-36] and these show similar behavior to those with L^1 (Figure S1), with an energy minimum at an average metal-donor distance of 2.63 Å. Therefore, the complexation of Mn^{2+} by L^3 induces a negligible amount of steric strain (approx. 3 kJ/mol), confirming the ideal cavity size for this metal ion.

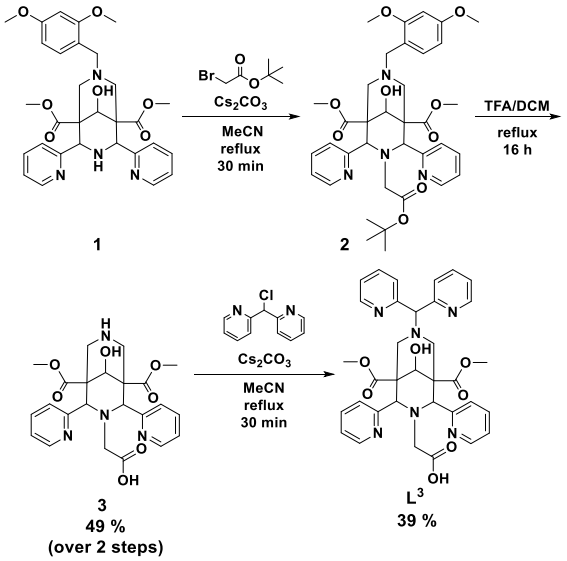

Scheme 2. Synthesis of L^3, starting from the known intermediate 1.[37]

Table 1. Selected bond lengths (Å) and angles (°) of $[MnL^3(MeOH)](OTf)_2$ in comparison to $[MnL^1(OTf)](OTf)$ and $[MnL^2](OTf)$.

	$[MnL^3(MeOH)](OTf)_2$	$[Mn(OTf)L^1](OTf)$[a]	$[MnL^2](OTf)$[a]
Bond [Å]			
M-N3	2.503(3)	2.4527(17)	2.3593(15)
M-N7	2.358(3)	2.4079(16)	2.5523(15)
M-Npy1	2.373(3)	3.037(2)	2.3635(18)
M-Npy2	2.353(4)	2.2937(19)	2.9098(22)
M-D(N3)	2.370(3)	2.2728(18)	2.2412(17)
M-Ndpy1	2.620(3)	2.2520(18)	2.4233(17)
M-Ndpy2	2.496(3)	2.5487(17)	2.3775(18)
M-O_x	2.182(3)	2.3804(16)	2.2018(14)
Angle [°]			
N3-M-N7	75.26(10)	72.42(5)	73.37(5)
Npy1-Mn-Npy2	131.52(11)	130.92(6)	129.37(5)

[a] ref.[25]

a)

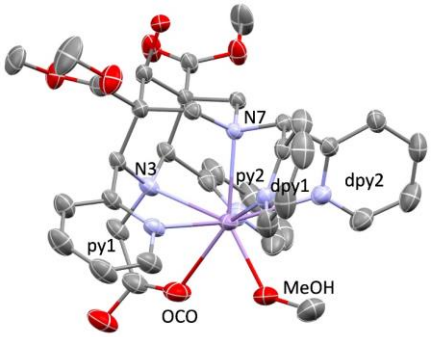

$[Mn(MeOH)L^2](OTf)_2 \cdot 2\ MeOH$

b)

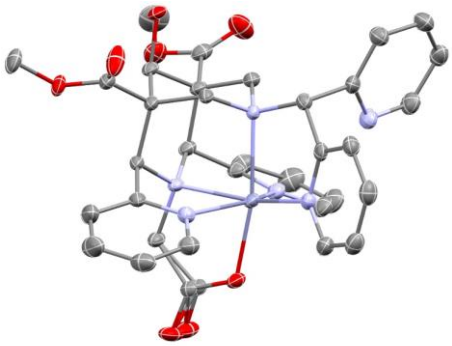

$[ZnL^2]OTf$

c)

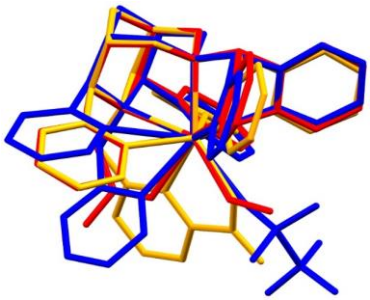

Figure 1. Plots of the solid state structures of a) $[MnL^3(MeOH)](OTf)_2$ and b) $[ZnL^3](OTf)$. Atoms shown at 50 % probability, hydrogen atoms, solvent molecules and anions have been omitted for clarity; c) overlay plot of the structures of the Mn^{II} complex cations with ligands L^1 (blue), L^2 (yellow), and L^3 (red); substituents to the bispidine backbone have been omitted.

Stability and kinetic inertness

In aqueous solution, pH-potentiometry was used to determine the protonation constants of L^3 and the thermodynamic stability constant and protonation constants of ZnL^3 (Figure S2, Table 2). In the Zn^{2+}-L^3 system, the species distribution curves corroborate the pH-dependent ^1H NMR data recorded in aqueous solution (Figure S3). Changes in the ^1H NMR spectra (in particular the chemical shift of the proton on the carbon bearing the two pyridines) correspond to pH regions where formation of the protonated (pH 0-3) or deprotonated complexes (pH 8-11) occur. The stability of the MnL^3 complex is too high to be assessed by potentiometry (the complex is fully formed at pH 2). Therefore, a relaxometric titration was done as previously described in batch samples between 0.8 M acid concentration and pH 10 to determine $\log K_{MnL}$ and $\log K_{MnHL}$ (Figure 2).[25] We note that the relaxivity of the complex remains stable even in basic pH (for >50 hours at pH 9) excluding hydrolysis of the ester groups. MnL^3 has a remarkably high stability constant, and the ligand retains good selectivity for Mn^{2+}, although the K_{MnL}/K_{ZnL} ratio is slightly lower than for L^1 and L^2. For ZnL^3, the high value of the first protonation constant ($\log K_{ZnHL} = 9.73$) shows that one tertiary amine remains protonated until basic pH, implying that this donor group is not coordinated to the metal ion, and this is also responsible for the reduced stability in comparison to the Mn^{2+} analogue. The pMn=9.82 value (pM= -log[Mn]$_{free}$, calculated for $c_{Mn}=c_L=10^{-5}$ M, pH 7.4) of MnL^3 is remarkably high and, apart from that for MnL^1, it is the highest ever reported for an Mn^{2+} complex with a coordinated H_2O molecule.

Because in ZnL^3 not all ligand donor groups are involved in the complexation, the formation of a dinuclear Zn_2L^3 complex might occur. Potentiometric titration of the ligand in presence of two equivalents of Zn^{2+} allowed to estimate the stability constant for Zn_2L^3 ($\log\beta_{Zn2L3} = 19.8(3)$; $\log\beta_{Zn2HL3} = 27.3(4)$). In contrast, no dinuclear complex is formed in the Mn^{2+}-L^3 system (see Supporting Information), and this was expected since Mn^{2+} coordinates to all donor groups of the ligand.

Table 2. Ligand protonation constants, Mn^{2+} and Zn^{2+} stabilities and pM values for the bispidine and reference ligands; errors in parenthesis are one standard deviation; I = 0.15 M NaCl, 298 K.

	L^1 [a]	L^2 [a]	L^3	L^4 [b]	PyC3A[c]	PC2A-EA [d]
$\log K_{H1}$	>11.05	11.90	12.26(3)	11.44	10.16	11.34
$\log K_{H2}$	6.73	5.44	6.52(2)	10.31	6.39	8.93
$\log K_{H3}$	5.62	5.28	4.41(2)	4.71	3.13	6.91
$\log K_{H4}$	5.27	1.36	2.83(3)	2.76	-	1.97
$\log K_{H5}$	2.30	-	-	2.22	-	-
$\log K_{MnL}$	24.2[a]	24.7[e]	19.47(2)[e]	12.21	14.14	19.01
$\log K_{MnHL}$	3.0	-	4.4(1)[e,f]	10.42	2.43	6.88
$\log K_{MnH2L}$	-	-	-	3.87	-	2.50
$\log K_{ZnL}$	14.30	14.70	15.04(6)	15.59	-	-
$\log K_{ZnHL}$	8.88	9.36	9.73(5)	10.33	-	-
$\log K_{ZnH2L}$	5.44	-	2.91(6)	3.28	-	-
p*Mn*[b]	12.71	12.59	9.82	6.65	8.17	9.27
p*Zn*[b]	9.50	8.58	8.73	8.40	-	-

[a] ref. [25]; [b] ref. [26]; [c] ref.[6]; [d] ref. [8]; [e] from relaxometric data. [f] $\log K_{MnHL} = 3.47(2)$ is obtained from titration of fully formed MnL^3 with HCl.

The kinetic inertness of Mn^{2+} complexes is typically assessed in trans-metalation experiments. Despite the four orders of magnitude difference between K_{MnL} and K_{ZnL}, due to the formation of the dinuclear complex Zn_2L^3, trans-metalation is shown to occur in presence of a sufficient excess of Zn^{2+}. This allows to directly compare MnL^3 with previously reported Mn^{2+} complexes using the same standard protocol. A similar situation occurs with GdDTPA ($\log K_{GdDTPA} = 22.46$, $\log K_{ZnDTPA} = 18.29$ and $\log\beta_{Zn2DTPA} = 22.77$).[38] First, we followed trans-metalation in presence of 25 equivalents of Zn^{2+} (pseudo-first order conditions) at pH 6 and 37 °C (Figure 3a). Under these conditions, the calculated dissociation half-life is 14.3 days, considerably longer than $t_{1/2}$ = 54.4 h or 64.5 h, reported for the most inert non-bispidine monohydrated complexes MnPC2A-EA[8] and MnPC2A-DPA.[20]

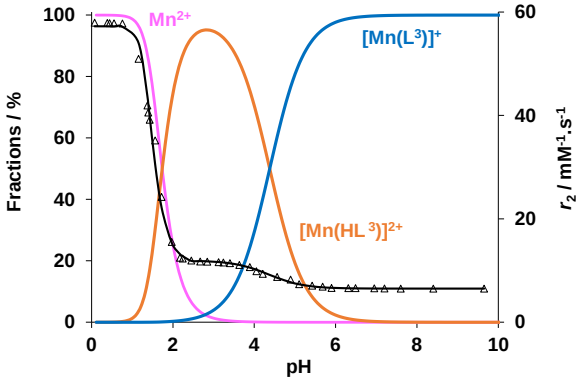

Figure 2. Species distribution curves calculated for MnL^3 (1 mM), and pH-dependent relaxivities (Δ) measured at 25 °C, 60 MHz. The black line represents the fit to yield stability constants.

In order to gain more insight into the mechanism of the slow dissociation, we have followed the reaction at varying concentrations of Zn^{2+} (10-50 equivalents) and varying pH (3.0-6.0). The pseudo-first order rate constants show a linear dependence on the Zn^{2+} concentration, while they are strictly independent of pH (Figure 3b). This unusual behavior implies that proton-assisted dissociation is negligible in this pH range, in sharp contrast to typical poly(amino carboxylate) metal complexes, for which it constitutes a major dissociation pathway. H^+-assisted demetalation is also observed for the Mn^{2+} complex of the pentadentate bispidine L^4.[26] The fit of the data in Figure 3b to $k_{obs} = k_0 + k_{Zn}$ [Zn] yields $k_{Zn} = (1.71\pm0.03)\times10^{-5}$ $M^{-1}s^{-1}$ for the rate constant of the metal-assisted dissociation. k_0, characteristic for the spontaneous dissociation could not be determined and had to be fixed to zero, otherwise a negative value was obtained with a large error, $k_0 = (-1\pm4)\times10^{-8}$ s^{-1}. Similar pH-invariance has been observed for MnL^1 dissociation in presence of excess Cu^{2+},[25] indicating that this peculiar behavior is characteristic for this family of octa-coordinate bispidine Mn^{2+} complexes. By considering solely the Zn^{2+}-assisted dissociation pathway, one can estimate a dissociation half-life of 4.7×10^4 days for physiological Zn^{2+} concentration (10 μM in the blood).[39] Although it is likely that under physiological conditions spontaneous dissociation has a more important role – it might even become the major contributor to dissociation – the estimated highest limit for k_0 in the order of 10^{-8} s^{-1} would correspond to a dissociation half-life of 82 days; hence one can conclude that MnL^3 has extremely high kinetic inertness.

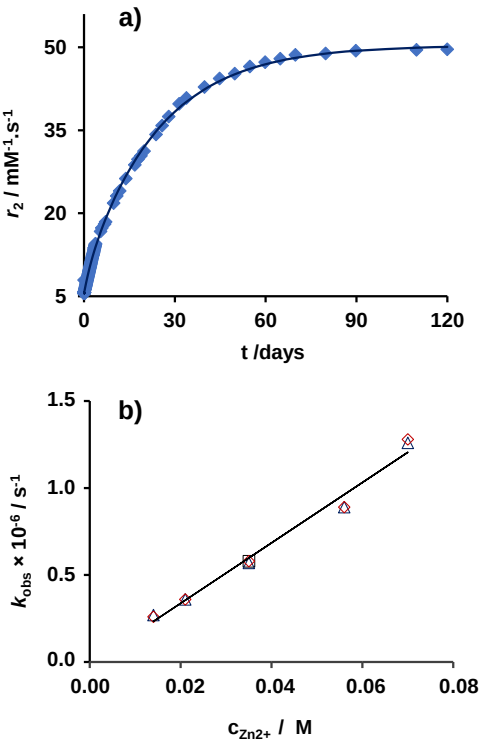

Figure 3. a) Time-dependent variation of the transverse ^1H relaxation rates in 1.4 mM MnL^3, 37°C, 60 MHz, 0.1 M NaCl, in the presence of 25 equivalents of Zn^{2+}. The curve represents the fit of the experimental data to yield the rate constant, k_{obs}. b) Variation of k_{obs} in Zn^{2+} trans-metalation experiments as a function of Zn^{2+} concentration. □ : pH 6.0 ; ◊ : pH 4.9; Δ : pH 3.1. c_{MnL} = 1.4 mM, 37 °C.

Complexation of L^3 with Mn^{2+} is relatively slow, but orders of magnitude faster than decomplexation. This indicates that there is no microscopic reversibility, i.e. complex formation and metal ion release follow different pathways. Especially for bispidine complexes, this is a common observation.[37, 40] Non-reversibility has also been observed when we have carried out a titration of fully formed MnL^3 (pH 7) with HCl (Fig. S3). The analysis of this curve yields a protonation constant of $\log K_{HMnL}$ = 3.47(2), around one log*K* unit below that determined from the relaxometric stability study (Table 2). Our interpretation of this important property for imaging applications, consistent with all observations, is based on two features of multidentate bispidine ligands: the rigidity of the chair-chair conformation of the bispidine backbone with the lone pairs of the two tertiary amines pointing to the center of the cavity, and the efficient encapsulation of the metal center. Due to the orientation of the lone pairs of the tertiary amines and the rigidity of the adamantane-derived backbone, bispidines are proton sponges,[28] and this also emerges from the high values of the first protonation constants (see Table 2). This is a reason for relatively slow complexation, depending on the metal ion, specific ligand and reaction conditions: the most demanding step is the deprotonation of the second tertiary amine, and in a number of examples, this has led to fast formation of relatively stable intermediates[41] in which the metal has not yet fully entered the bispidine cavity. Such a pre-complex has also been identified in the formation of MnL^1 and its stability constant could be determined.[25] Once the

complex is formed, there is no possibility of competing protonation – the metal ion is completely locked in the bispidine cavity – in this sense, one might think of bispidines as "metal ion sponges". The fact that the pendant donor groups are well oriented and resistant to H^+-assisted decomplexation is also illustrated by the structure of MnL^3, where protonation of the acetate group does not lead to partial decomplexation (see above). The attack of OH^- is another potential decomplexation pathway, a process that may become increasingly prevalent at higher pH and when the complex concentration is very low with respect to the OH^- concentration (e.g. in the case of radiotracer imaging, typically used at subnanomolar concentrations). In our case, the complex remains intact even at pH 10 for several days, as followed by relaxometric measurements. Therefore, we conclude that very efficient encapsulation by the heptacoordinate ligand L^3 completely shields the metal ion from attack by OH^-. Finally, we also note that the slow formation of such Mn^{2+} bispidine complexes is not expected to constitute an obstacle for their potential large-scale production.

Relaxation properties

The solid-state structure of MnL^3 shows the coordination of one solvent methanol in the inner sphere of Mn^{2+}, which is certainly replaced by a water molecule in aqueous solution. This was indeed confirmed by measuring the temperature-dependent ^{17}O transverse relaxation rates ($1/T_2$) and using the method of Gale to estimate the hydration number,[42] which gave q = 1.0 (Fig. S7).

The relaxivity of MnL^3 amounts to r_1 = 4.44 $mM^{-1}s^{-1}$ (25 °C, 20 MHz), very close to that of commercial agents based on Gd^{3+} (r_1 = 4.74 $mM^{-1}s^{-1}$ for GdDOTA).[43] The relaxivity is slightly higher than that of $MnHL^4$ (r_1 = 4.28 $mM^{-1}s^{-1}$) and ~30 % higher than for typical monohydrated Mn^{2+} complexes formed with non-bispidine chelators[44] (e.g. MnPyC3A: 3.3 $mM^{-1}s^{-1}$, MnPC2A-EA: 3.52 $mM^{-1}s^{-1}$; Mn(1,4-DO2A): 2.1 $mM^{-1}s^{-1}$). In the presence of human serum albumin, the relaxivity of MnL^3 increases (by ~40 % at 20 MHz, 25 °C), indicating some non-specific protein binding, which is likely induced by the presence of the pyridine pendants (Figure 4a).

The relaxation efficiency of MnL^3 has been further characterized by recording Nuclear Magnetic Relaxation Dispersion (^1H NMRD) profiles at 25°C and 37°C, from 0.01 to 80 MHz (Figure 4a). The shape and temperature dependence of these profiles are characteristic for small molecular weight complexes and indicate that the relaxivity is limited by fast motional dynamics. Direct information on the water exchange has been obtained from the analysis of the variable temperature ^{17}O relaxation rates (Figure 4b). These were fitted together with the NMRD profiles to yield parameters characterizing the water exchange and rotational dynamics of MnL^3, as shown in Table 3 (see Supporting Information for full details). The water exchange rate constant for MnL^3, k_{ex}^{298}, is about twice as high as for $MnHL^4$. While this increase has no impact on the relaxivity, it is interesting to note that it is accompanied by a change of the exchange mechanism, associative for the six-coordinate $MnHL^4$ and dissociative for the eight-coordinate MnL^3: the activation entropy ($\Delta S^{\neq}$) is positive for MnL^3 and negative for $MnHL^4$. This also supports the hypothesis discussed above that in MnL^3 the metal center is completely shielded from attack of other ligands (especially OH_2 and OH^-), while for systems with lower coordination numbers this is not the case.

The slight relaxivity increase for MnL^3 as compared to $MnHL^4$ can be attributed to its slightly higher molecular weight (17%), thus slower rotational motion, as reflected by the rotational correlation time determined in the fit (Table 3). This compensates the lack of the second-sphere relaxation mechanism, which is operating for $MnHL^4$, thanks to the presence of the charged non-coordinating carboxylate groups but missing for the ester-bearing MnL^3.

In vivo and ex vivo studies

Given the excellent Mn^{2+}/Zn^{2+} selectivity and kinetic inertness of MnL^3 combined with relaxivities that clearly outstrip those typically reported for small Mn^{2+} complexes, we carried out a standard *in vivo* MRI study (7 T) in wild type mice. Mice were injected intravenously with a solution of MnL^3 at a 0.02 mmol/kg dose, 80 % lower than that used in the clinic. The MR images obtained show very good contrast at the level of the kidneys 2 min after injection. No significant liver uptake is noted. Overall, these images illustrate the high relaxation efficiency of MnL^3, which is retained *in vivo*. The normalized signal intensities followed for one-hour post-injection in the kidney, the liver and the aorta are shown in Figure 5. The highest signal intensity was reached at ~5 mins after injection. These kinetic data point to a rapid and primarily renal elimination of the compound. The biodistribution half-life of MnL^3 in the kidney was estimated to 25 min, a value similar to that of clinically used small contrast agents.

Complete elimination of the probe from the mice was confirmed by an *ex vivo* biodistribution study. Mice were sacrificed at 24 h post injection (0.02 mmol/kg dose MnL^3) and the organs harvested. The manganese content was determined by ICP-MS in different organs following acid digestion. The results obtained (Table 4) are compared with baseline values from the literature[45] or determined by us, and with those reported for a PyC3A-derivative-based Mn^{2+} complex[18] developed for liver imaging (Table 4). 24 h after injection, MnL^3 is completely excreted from the body.

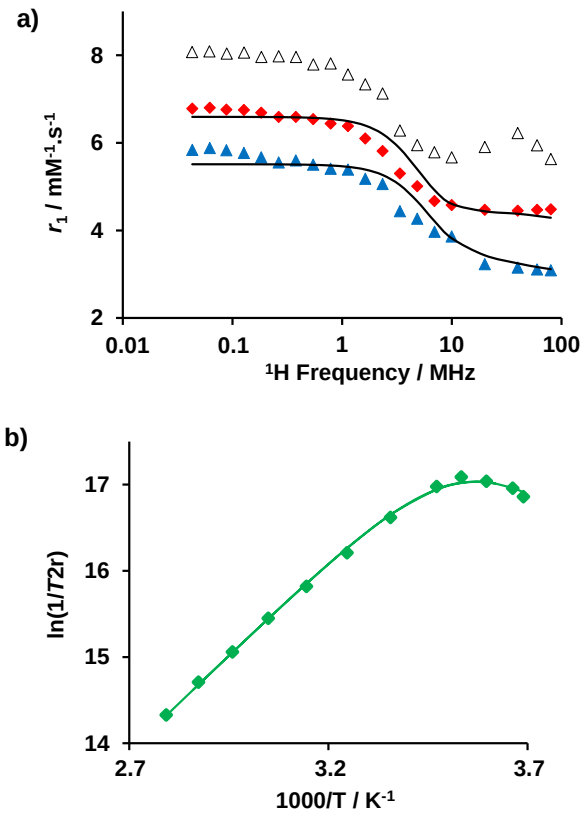

Figure 4. a) Proton relaxivities of MnL^3 measured in water at 25°C (♦) and 37 °C (▲) and in human serum at 37 °C (Δ), and b) reduced transverse ^{17}O relaxation rates (♦; 9.4 T). The lines represent the simultaneous fit of the experimental points using the Solomon-Bloembergen-Morgan theory of paramagnetic relaxation.

Table 3. Parameters characterizing water exchange and rotational dynamics obtained from the analysis of ^1H NMRD and ^{17}O NMR data.

	MnL^3	MnPyC3A[a]	MnPC2A-EA[b]	Mn(1,4-DO2A)[c]
q	1	1	1	0.9
r_1 ($mM^{-1}s^{-1}$)	3.17[d]/4.44[e]	2.1[d]	3.5[f]	1.7[d]
k_{ex}^{298} (10^7 s^{-1})	13.5(5)[g]	5.4	4.0	113.4
$\Delta H^{\neq}$ ($kJmol^{-1}$)	34.0(6)	37.2	-	29.4
$\Delta S^{\neq}$ ($Jmol^{-1}K^{-1}$)	+25(12)	-	-	-
E_{rH} ($kJ.mol^{-1}$)	22(3)	-	-	19.1
τ_{rH}^{298} (ps)	110(4)	-	-	46

a. ref.[6] b. ref. [8] c. ref. [23] d. 37 °C, 60 MHz. e. 25 °C, 20 MHz. f. 25 °C, pH 6, 20 MHz. g. The scalar coupling constant calculated from the fit of ^{17}O NMR data is $A_o/\hbar$ = 30.3(5)×10^6 $rad.s^{-2}$

Table 4. Mn tissue content determined by ICP-MS in wild type 8-weeks-old C57BL/6JRj mice, 24 h post injection of 0.02 mmol/kg of MnL^3. Data are presented as nmol/g ± SD (n = 3).

	MnL^3	Mn(PyC3A-OBn)[18] [a]	baseline (no injection)	baseline[45]
lungs	3.3±0.3	4.87	3.5±0.2	1.8
liver	20.4±4.0	23.3	14.1±1.2	16.5
spleen	2.2±0.9	9.03	1.8±0.6	2.2
kidneys	19.6±3.4	31.6	26.2±0.6	18.9

[a] in balb/C mice; 0.1 mmol/ kg injected dose

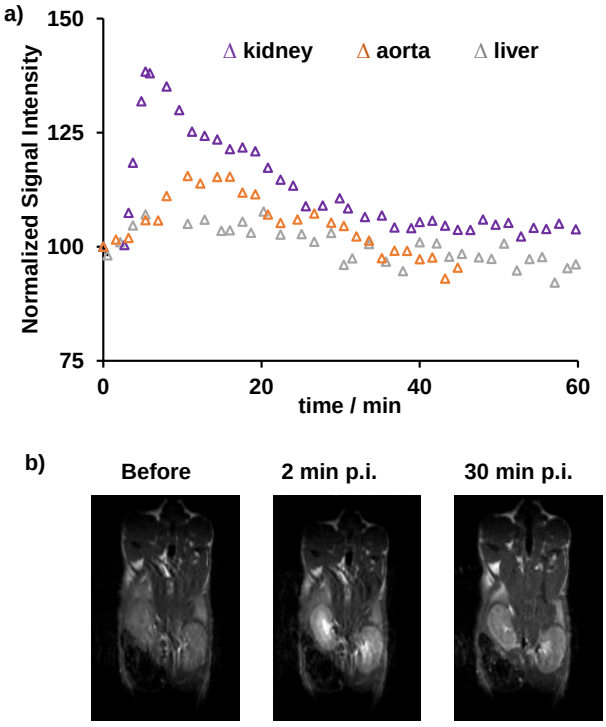

Figure 5. a) Normalized signal intensity in the kidney, liver and aorta plotted as a function of time. Measurements were performed for 3 mice. Standard deviations are not presented for better readability. b) Coronal T1-weighted MR images prior to injection and at 2 and 30 min post intravenous injection of 0.02 mmol/kg of MnL^3.

CONCLUSION

In conclusion, rational chemical design has provided a small molecular weight Mn^{2+} complex combining unique features highly relevant for the development of more biocompatible alternatives to Gd^{3+}-based MRI agents. The remarkably high thermodynamic stability, Mn^{2+}/Zn^{2+} selectivity and resistance to dissociation, all related to the rigidity, size-match and full encapsulation of MnL^3, are decisive to avoid *in vivo* free metal ion release. Despite the seven ligand donor atoms, the large coordination cavity also affords for an inner sphere coordinated water in the complex, which, together with the slightly elevated molecular size, leads to proton relaxivities ~30 % higher than those of typical Mn^{2+} complexes. *In vivo* in mice, MnL^3 retains this good relaxation efficiency, and undergoes rapid clearance mainly *via* the kidneys. Further improvement of the pharmacokinetic profile and the relaxivity can likely be achieved by substitution of the bispidine backbone, e.g. with carboxylates, phosphates or sulfonates, and simple synthetic protocols for such derivatives are available.[40, 46-47]

ASSOCIATED CONTENT

Supporting Information. Details of synthesis, experimental procedures, X-ray crystal structure determinations and hole-size calculations, potentiometric titration curves, kinetic and NMR data, description of the analysis of ^{17}O NMR and NMRD data. This material is available free of charge via the Internet at http://pubs.acs.org.

AUTHOR INFORMATION

Corresponding Author

* peter.comba@aci.uni-heidelberg.de; eva.jakabtoth@cnrs.fr

Author Contributions

The manuscript was written through contributions of all authors. All authors have given approval to the final version of the manuscript. ‡These authors contributed equally.

Funding Sources

Any funds used to support the research of the manuscript should be placed here (per journal style).

Notes

The authors declare no conflict of interest.

ACKNOWLEDGMENT

Financial support by Heidelberg University, the German Science Foundation (Deutsche Forschungsgemeinschaft, DFG) and CNRS France is gratefully acknowledged. This study was conducted within the Max Planck School Matter to Life, supported by the German Federal Ministry of Education and Research (BMBF) in collaboration with the Max Planck Society.

REFERENCES

1. Agarwal, R.; Brunelli, S. M.; Williams, K.; Mitchell, M. D.; Feldman, H. I.; Umscheid, C. A. Gadolinium-based contrast agents and nephrogenic systemic fibrosis: a systematic review and meta-analysis. *Nephrol. Dial. Transplant.* **2008,** *24*, 856.

2. Grobner, T. Gadolinium - a specific trigger for the development of nephrogenic fibrosing dermopathy and nephrogenic systemic fibrosis? *Nephrol. Dial. Transplant.* **2006,** *21*, 1104.

3. Di Gregorio, E.; Ferrauto, G.; Furlan, C.; Lanzardo, S.; Nuzzi, R.; Gianolio, E.; Aime, S. The Issue of Gadolinium Retained in Tissues: Insights on the Role of Metal Complex Stability by Comparing Metal Uptake in Murine Tissues Upon the Concomitant Administration of Lanthanum- and Gadolinium-Diethylentriamminopentaacetate. *Invest. Radiol.* **2018,** *53*, 167.

4. Kanal, E.; Tweedle, M. F. Residual or Retained Gadolinium: Practical Implications for Radiologists and Our Patients. *Radiology* **2015,** *275*, 630.

5. Gupta, A.; Caravan, P.; Price, W. S.; Platas-Iglesias, C.; Gale, E. M. Applications for Transition-Metal Chemistry in Contrast-Enhanced Magnetic Resonance Imaging. *Inorg. Chem.* **2020,** *59*, 6648.

6. Gale, E. M.; Atanasova, I. P.; Blasi, F.; Ay, I.; Caravan, P. A Manganese Alternative to Gadolinium for MRI Contrast. *J. Am. Chem. Soc.* **2015,** *137*, 15548.

7. Drahoš, B.; Lukeš, I.; Tóth, É. Manganese(II) Complexes as Potential Contrast Agents for MRI. *Eur. J. Inorg. Chem.* **2012,** *2012*, 1975.

8. Botár, R.; Molnár, E.; Trencsényi, G.; Kiss, J.; Kálmán, F. K.; Tircsó, G. Stable and Inert Mn(II)-Based and pH-Responsive Contrast Agents. *J. Am. Chem. Soc.* **2020,** *142*, 1662.

9. Forgacs, A.; Pujales-Paradela, R.; Regueiro-Figueroa, M.; Valencia, L.; Esteban-Gomez, D.; Botta, M.; Platas-Iglesias, C. Developing the family of picolinate ligands for Mn(2+) complexation. *Dalton Trans.* **2017,** *46*, 1546.

10. Forgacs, A.; Regueiro-Figueroa, M.; Barriada, J. L.; Esteban-Gomez, D.; de Blas, A.; Rodriguez-Blas, T.; Botta, M.; Platas-Iglesias, C. Mono-, bi-, and trinuclear bis-hydrated Mn(2+) complexes as potential MRI contrast agents. *Inorg. Chem.* **2015,** *54*, 9576.

11. Molnar, E.; Camus, N.; Patinec, V.; Rolla, G. A.; Botta, M.; Tircso, G.; Kalman, F. K.; Fodor, T.; Tripier, R.; Platas-Iglesias, C. Picolinate-containing macrocyclic Mn2+ complexes as potential MRI contrast agents. *Inorg. Chem.* **2014,** *53*, 5136.

12. Molnar, E.; Varadi, B.; Garda, Z.; Botar, R.; Kalman, F. K.; Tóth, É.; Platas-Iglesias, C.; Toth, I.; Brucher, E.; Tircso, G. Remarkable differences and similarities between the isomeric Mn(II)-cis- and trans-1,2-diaminocyclohexane-N,N,N ',N '-tetraacetate complexes. *Inorg. Chim. Acta* **2018,** *472*, 254.

13. Pota, K.; Garda, Z.; Kalman, F. K.; Barriada, J. L.; Esteban-Gomez, D.; Platas-Iglesias, C.; Toth, I.; Brucher, E.; Tircso, G. Taking the next step toward inert Mn2+ complexes of open-chain ligands: the case of the rigid PhDTA ligand. *New J. Chem.* **2018,** *42*, 8001.

14. Regueiro-Figueroa, M.; Rolla, G. A.; Esteban-Gomez, D.; de Blas, A.; Rodriguez-Blas, T.; Botta, M.; Platas-Iglesias, C. High Relaxivity Mn2+-Based MRI Contrast Agents. *Chem. Eur. J.* **2014,** *20*, 17300.

15. Erstad, D. J.; Ramsay, I. A.; Jordan, V. C.; Sojoodi, M.; Fuchs, B. C.; Tanabe, K. K.; Caravan, P.; Gale, E. M. Tumor Contrast Enhancement and Whole-Body Elimination of the Manganese-Based Magnetic Resonance Imaging Contrast Agent Mn-PyC3A. *Invest. Radiol.* **2019,** *54*, 697.

16. Gale, E. M.; Mukherjee, S.; Liu, C.; Loving, G. S.; Caravan, P. Structure–Redox–Relaxivity Relationships for Redox Responsive Manganese-Based Magnetic Resonance Imaging Probes. *Inorg. Chem.* **2014,** *53*, 10748.

17. Gale, E. M.; Wey, H.-Y.; Ramsay, I.; Yen, Y.-F.; Sosnovik, D. E.; Caravan, P. A Manganese-based Alternative to Gadolinium: Contrast-enhanced MR Angiography, Excretion, Pharmacokinetics, and Metabolism. *Radiology* **2018,** *286*, 877.

18. Wang, J.; Wang, H.; Ramsay, I. A.; Erstad, D. J.; Fuchs, B. C.; Tanabe, K. K.; Caravan, P.; Gale, E. M. Manganese-Based Contrast Agents for Magnetic Resonance Imaging of Liver Tumors: Structure-Activity Relationships and Lead Candidate Evaluation. *J. Med. Chem.* **2018,** *61*, 8811.

19. Botta, M.; Carniato, F.; Esteban-Gomez, D.; Platas-Iglesias, C.; Tei, L. Mn(II) compounds as an alternative to Gd-based MRI probes. *Fut. Med. Chem.* **2019,** *11*, 1461.

20. Botár, R.; Molnár, E.; Garda, Z.; Madarasi, E.; Trencsényi, G.; Kiss, J.; Kálmán, F. K.; Tircsó, G. Synthesis and characterization of a stable and inert MnII-based ZnII responsive MRI probe for molecular imaging of glucose stimulated zinc secretion (GSZS). *Inorg. Chem. Front.* **2022,** *9*, 577.

21. Kálmán, F. K.; Nagy, V.; Váradi, B.; Garda, Z.; Molnár, E.; Trencsényi, G.; Kiss, J.; Même, S.; Même, W.; Tóth, É.; Tircsó, G. Mn(II)-Based MRI Contrast Agent Candidate for Vascular Imaging. *J. Med. Chem.* **2020,** *63*, 6057.

22. Garda, Z.; Forgács, A.; Do, Q. N.; Kálmán, F. K.; Timári, S.; Baranyai, Z.; Tei, L.; Tóth, I.; Kovács, Z.; Tircsó, G. Physico-chemical properties of Mn-II complexes formed with cis- and trans-DO2A: thermodynamic, electrochemical and kinetic studies. *J. Inorg. Biochem.* **2016,** *163*, 206.

23. Rolla, G. A.; Platas-Iglesias, C.; Botta, M.; Tei, L.; Helm, L. H-1 and O-17 NMR Relaxometric and Computational Study on Macrocyclic Mn(II) Complexes. *Inorg. Chem.* **2013,** *52*, 3268.

24. https://clinicaltrials.gov/ct2/show/NCT05413668 date of access: 13 October 2022.

25. Cieslik, P.; Comba, P.; Dittmar, B.; Ndiaye, D.; Tóth, É.; Velmurugan, G.; Wadepohl, H. Exceptional Manganese(II) Stability and Manganese(II)/Zinc(II) Selectivity with Rigid Polydentate Ligands. *Angew. Chem. Int. Ed.* **2022,** *61*, e202115580.

26. Ndiaye, D.; Sy, M.; Pallier, A.; Même, S.; de Silva, I.; Lacerda, S.; Nonat, A. M.; Charbonnière, L. J.; Tóth, É. Unprecedented Kinetic Inertness for a Mn2+-Bispidine Chelate: A Novel Structural Entry for Mn2+-Based Imaging Agents. *Angew. Chem. Int. Ed.* **2020,** *59*, 11958.

27. Sy, M.; Ndiaye, D.; da Silva, I.; Lacerda, S.; Charbonniere, L. J.; Tóth, É.; Nonat, A. M. 55/52Mn2+ Complexes with a Bispidine-Phosphonate Ligand: High Kinetic Inertness for Imaging Applications. *Inorg. Chem.* **2022,** *61*, 13421.

28. Comba, P.; Kerscher, M.; Schiek, W., Bispidine Coordination Chemistry. In *Progress in Inorganic Chemistry, Vol 55*, Karlin, K. D., Ed. 2007; Vol. 55, pp 613.

29. Comba, P.; Schiek, W. Fit and misfit between ligands and metal ions. *Coord. Chem. Rev.* **2003,** *238-239*, 21.

30. Dube, K. S.; Harrop, T. C. Structure and properties of an eight-coordinate Mn(II) complex that demonstrates a high water relaxivity. *Dalton Trans.* **2011,** *40*, 7496.

31. Dang, D.; Bai, Y.; Duan, C. Crystal structure and magnetic properties of a novel octa-coordinated manganese(II) complex. *J. Chem. Cryst.* **2008,** *38*, 557.

32. Reid, H. O. N.; Kahwa, I. A.; White, A. J. P.; Williams, D. J. Intense photosensitized emission from stoichiometric compounds featuring Mn2+ in seven- and eightfold coordination environments. *Inorg. Chem.* **1998,** *37*, 3868.

33. Neupertlaves, K.; Dobler, M. Crystal-structure of metal-ion complexes with neutral noncycluc ionophores. *Helv. Chim. Acta* **1977,** *60*, 1861.

34. Comba, P.; Okon, N.; Remenyi, R. Computation of cavity shapes, sizes and plasticities. *J. Comput. Chem.* **1999,** *20*, 781.

35. Comba, P.; Hambley, T. W.; Strohle, M. The directionality of d-orbitals and molecular-mechanics calculations of octahedral transition-metal compounds. *Helv. Chim. Acta* **1995,** *78*, 2042.

36. Comba, P.; Hambley, T. W.; Lauer, G.; Okon, N., *MOMEC97, a molecular modeling package for inorganic compounds*. Heidelberg, Germany, 1997.

37. Comba, P.; Jermilova, U.; Orvig, C.; Patrick, B. O.; Ramogida, C. F.; Rück, K.; Schneider, C.; Starke, M. Octadentate Picolinic Acid-Based Bispidine Ligand for Radiometal Ions. *Chem. Eur. J.* **2017,** *23*, 15945.

38. Sarka, L.; Burai, L.; Brucher, E. The rates of the exchange reactions between GdDTPA and the endogenous ions Cu2+ and Zn2+: A kinetic model for the prediction of the in vivo stability of GdDTPA, used as a contrast agent in Magnetic Resonance Imaging. *Chem. Eur. J.* **2000,** *6*, 719.

39. May, P. M.; Linder, P. W.; Williams, D. R. Computer Simulation of Metal ion equilibria in biofluids: Models for the Low-molecular-weight comlex distribution of Calcium(II), Magnesium(II), Manganese(II), Iron(III), Copper(II), Zinc(II), and Lead(II) ions in human blood plasma. *J.Chem.Soc.; Dalton Trans.* **1977,** 588.

40. Comba, P.; Kerscher, M.; Rück, K.; Starke, M. Bispidines for radiopharmaceuticals. *Dalton Trans.* **2018,** *47*, 9202.

41. Bruchertseifer, F.; Comba, P.; Martin, B.; Morgenstern, A.; Notni, J.; Starke, M.; Wadepohl, H. First-Generation Bispidine Chelators for Bi-213(III) Radiopharmaceutical Applications. *Chemmedchem* **2020,** *15*, 1591.

42. Gale, E. M.; Zhu, J.; Caravan, P. Direct Measurement of the Mn(II) Hydration State in Metal Complexes and Metalloproteins through O-17 NMR Line Widths. *J. Am. Chem. Soc.* **2013,** *135*, 18600.

43. Powell, D. H.; Ni Dhubhghaill, O. M.; Pubanz, D.; Lebedev, Y.; Schlaepfer, W.; Merbach, A. E. Structural and Dynamic Parameters Obtainde from 17O NMR, EPR, and NMRD Studies of Monomeric and Dimeric Gd3+ Complexes of Interest in Magnetic Resonance Imaging: An Integrated and Theoretically Self-Consistent Approach. *J. Am. Chem. Soc.* **1996,** *118*, 9333.

44. Lacerda, S.; Ndiaye, D.; Tóth, É., MRI relaxation agents based on transition metals. In Hubbard, C. D.; Van Eldik, R., Eds. *Advances in Inorganic Chemistry, Recent Highlights I*, Vol. 78, Elsevier, 2021.

45. Seo, Y. A.; Elkhader, J. A.; Wessling-Resnick, M. Distribution of manganese and other biometals in flatiron mice. *Biometals* **2016,** *29*, 147.

46. Abad-Galán, L.; Cieslik, P.; Comba, P.; Gast, M.; Maury, O.; Neupert, L.; Roux, A.; Wadepohl, H. Excited State Properties of Lanthanide(III) Complexes with a Nonadentate Bispidine Ligand. *Chem. Eur. J.* **2021,** *27*, 10303.

47. Comba, P.; Morgen, M.; Wadepohl, H. Tuning of the Properties of Transition-Metal Bispidine Complexes by Variation of the Basicity of the Aromatic Donor Groups. *Inorg. Chem.* **2013,** *52*, 6481.

Insert Table of Contents artwork here